Numerical model for noise reduction of small vertical-axis wind turbines

Wen-Yu Wang[1], Yuh-Ming Ferng[2]

[1] Department of Green Energy, National University of Tainan, Tainan City, Taiwan

[2] Department of Engineering and System Science, National Tsing Hua University, Hsinchu City, Taiwan

5   *Correspondence to*: Wen-Yu Wang (wywang@mail.nutn.edu.tw)

Abstract. Wind turbines are a promising solution for sustainable energy, but their noise emissions present a challenge to public acceptance. Numerous blade designs have been aimed at reducing noise but often come with a decrease in wind turbine aerodynamic efficiency. In this study, the acoustic power and torque of a 5 kW vertical-axis wind turbine (VAWT) were simulated by using different mesh sizes and turbulence models.

10 The simulated torque and noise of the turbine have significant sensitivity to the mesh size, so suitable mesh sizes were determined for the near-wall and rotating regions that can be used as a design reference for future turbines with similar operating conditions. The selection of the turbulence model was found to affect the predicted torque by about 10% and the predicted tip noise by about 2 dB. The selected mesh size and turbulence model were then applied to simulating the effectiveness of three common noise mitigation

15 techniques: a mask, deflector, and wall roughness. The results showed that deflectors are suitable for noise reduction of small VAWTs. This paper provides valuable information on simulating noise propagation from small VAWTs and the optimal noise reduction techniques.

1. Introduction

Taiwan has poor petrochemical energy resources and relies on imports to meet about 98% of its energy
20 needs. Thus, the active development of green energy has become an increasingly important issue. Owing to Taiwan's geography and monsoon climate, large amounts of wind energy are available. Wind power generation offers significant environmental benefits and is a feasible option as a renewable energy resource. Advances in aerodynamics theory, materials, and manufacturing technologies have improved the performance and reliability of wind turbines while lowering the cost of electricity generation. Around the
25 world, the rise of high-density cities has led to a gradual increase in high-rise buildings, which has increased interest in wind energy for urban environments. A vertical-axis wind turbine (VAWT) offers less power than the conventional horizontal-axis wind turbine, but it has a simple design, can operate at low wind speeds, and has low noise emissions. Thus, VAWTs are suitable for urban environments with many buildings. The global installed capacity of small wind turbines in urban areas has been growing annually since 2010 and reached
30 1427.5 MW in 2020 (Li et al., 2022). However, the spread of wind power generation is limited not only by the terrain but also by the noise generated by the wind and turbine blades, which may affect nearby residents. During operation, a wind turbine can produce about 95 sound pressure level (dB) of noise, which gradually decreases with increasing distance to an acceptable level of 40 dB at 300 m or more. Therefore, wind turbines generally need to be constructed at least 300 m away from residential areas.
35 The analysis of noise by air is a mature research topic. Lighthill (1952) derived an acoustic wave equation by using fluid mechanics theory, where the sound source term can be obtained experimentally or by computational fluid dynamics (CFD). The method of separating the flow and sound fields for analysis is called the acoustic analogy theory. Proudman et al. (1952) improved upon Lighthill's work and derived the sound source caused by isotropic turbulence. Pradera et al. (2007) calculated various aerodynamic parameters
40 and noise generated by viscous fluids with low and high Reynolds numbers passing over a cylinder and used the Ffowcs Williams–Hawkings (FW–H) equation to predict the sound pressure, which they then transformed into the sound pressure level through the fast Fourier transform for noise analysis. Their analytical results showed good agreement with the experimental data. Tadamasa et al. (2011) used the CFD software CFX to

analyze the NREL Phase VI blade and verified the aerodynamic coefficient by comparison with experimental
data from Sorensen et al. (2001).

Various experimental and numerical techniques have been developed for mitigating the noise emissions
of wind turbines based on their aero-acoustic characteristics. Some promising noise mitigation techniques
targeting dominant noise sources have been discussed, including reducing the inflow turbulence noise,
trailing edge noise, and tip noise. The tip noise is a dominant noise source of wind turbines. Maizi et al. (2018)
performed a numerical analysis showing that a shark tip reduced the tip noise by 7% compared with the
reference tip but with a tradeoff of 3% less power. However, their computational approach involved using a
detached eddy simulation to resolve the flow field and the FW–H equation for acoustic calculations, which
was very computationally intensive. Deshmukh et al. (2018) included the tip region in an annular domain for
a parametric study of blended winglets to evaluate the improvement in the aerodynamic and aero-acoustic
performances. Their methodology significantly reduced the computational cost, and their results showed that
noise emissions were reduced by about 25% at mid-high frequencies along with enhanced torque output.
Mohamed (2016) used a CFD model combined with an unsteady realizable k–ε turbulence model to analyze
the noise and efficiency of H-rotor Darrieus VAWT with different spacings at different velocity ratios. The
results showed that, compared with a single blade, a double blade with 60% spacing effectively reduced the
noise by 40% across the entire frequency range, but the efficiency and torque were decreased. In addition, an
excessively large or small spacing (e.g., 20% or 90%) increased noise emissions. Botha et al. (2017)
compared the noise emissions of a six-bladed 2 kW VAWT measured in experiments with the two-
dimensional analytical solution and the CFD predictions. Their results indicated that the CFD model was
reliable while the analytical solution fell short. They then applied the CFD results to improve the
dimensionless parameters of some analytical mathematical models and improve their accuracy. Naccache et
al. (2017) performed 2D experiments to verify their CFD model. The results showed that using a shear stress
transport SST k–ω turbulence model with a near-wall mesh of $y^+ < 15$ could accurately predict the lift
coefficient, lift–drag ratio, and power coefficient at different azimuth angles and rotational speed ratios. This
model was then applied to conducting in-depth 3D simulations. Naccache et al. (2018) showed the
Dual Vertical Axis Wind Turbine (D-VAWT) is an innovative turbine proposed to improve the aerodynamic
efficiency of small VAWTs. The D-VAWT has two axes, enabling the blades to move in an oval shaped path
and thereby expanding the region of maximum power generation of typical VAWTs. They also found that,
based on CFD simulations, the D-VAWT has relatively low sensitivity to the change of tip speed ratio
compared to VAWTs.

Previous studies numerically investigated the low-frequency emissions of a generic 5 MW wind turbine and
evaluated the influence of a tower and steady blade deformation under uniform inflow conditions. Klein et
al. (2018) coupled the CFD solver FLOWer to the multibody simulation (MBS) solver SIMPACK, which
they applied to minimizing the noise emissions of a wind farm by changing the operating modes of individual
wind turbines. Nyborg et al. (2023) showed that using a higher-fidelity sound propagation model such as
WindSTAR, over the simple ISO 9613-2 model, resulted in significant improvement in the noise-constrained
optimization of wind farms. Abreu et al. (2022) used advanced 3D numerical techniques to study whether
the ground structure on the wave path between a wind turbine and seismic station can be changed to reduce
or mitigate the noise emissions of the wind turbine. They showed that filling trenches with water and
relatively simple changes to the topography helped reduce noise emissions. Chen et al. (2021) designed two
types of deflectors to enhance the performance of a three-bladed VAWT and found that the optimized upper
deflector improved the performance by 20% and the optimized lower deflector improved the performance by
17%.

The objective of the present study was to analyze the noise emissions of a 5 kW VAWT and the effects of
different noise reduction techniques on not only the noise emissions but also the aerodynamic torque and
acoustic power. The effects of different steady-state turbulence models and the mesh size on the results were
evaluated, and the optimal mesh size and model were then applied to analyzing three different noise reduction
techniques. Overall, very few studies used Darrieus VAWT to simulate the noise emissions, however, noise

reduction techniques of the small-scale wind turbines are very limited. This study may contribute to the spread of small-scale wind turbines in an urban setting.

2. Methods

2.1 Numerical method

Blade design for small VAWTs must consider both the power generated and noise emitted. The CFD code, ANSYS FLUENT, is commercially available and an industrial leading software used to simulate the aerodynamic performance of wind turbine airfoils and aeroacoustic analysis. (Yao et al., 2012, Zaareer et al., 2023) In this study, ANSYS FLUENT was used to simulate turbulence and acoustic models to analyze the causes of noise emissions. The governing equations were as follows. The flow velocity was much less than the speed of sound, so the aerodynamic flow field can be considered incompressible. In addition, frictional heating is the only possible heat source and is extremely small, so the effect of thermal expansion and contraction on the density of the fluid can be neglected. Therefore, the continuity equation can be written as

$$\frac{\partial \rho}{\partial t} + \nabla \cdot (\rho v) = 0 \tag{1}$$

where ρ is the density and v is the velocity. The momentum equation is written as

$$\frac{\partial}{\partial x_i}(\rho u_i u_j) = -\frac{\partial P}{\partial x_i} + \frac{\partial \tau_{ij}}{\partial x_i} + \rho g_i \tag{2}$$

$$\tau_{ij} = (\mu + \mu_t)\frac{\partial u_i}{\partial x_j} \tag{3}$$

where P is the static pressure, τ_{ij} is the stress tensor, μ is the viscosity, μ_t is the turbulent viscosity, ρg_i is the body force, x_i is the x-coordinate, x_j is the y-coordinate, u_i is the x-component velocity, and u_j is the y-component velocity.

2.2 Turbulence models

Based on a review of relevant research, the realizable k–ε model and SST k–ω model were selected as turbulence models. These models modify their original two-equation versions to address phenomena such as vortices, wake flows, and flow separation. These models can be used to simulate the turbulence generated by a blade passing through the wind field reliably and economically. The realizable k–ε model is considered more accurate than the standard k–ε model at predicting the dissipation rate distribution and boundary layer characteristics of separated and recirculating flows. The turbulence kinetics is expressed as

$$\frac{\partial}{\partial t}(\rho k) + \frac{\partial}{\partial x_j}(\rho k u_j) = \frac{\partial}{\partial x_j}\left[\left(\mu + \frac{\mu_t}{\sigma_k}\right)\frac{\partial k}{\partial x_j}\right] + G_k + G_b - \rho \epsilon - Y_M + S_k \tag{4}$$

The dissipation rate is expressed as

$$\frac{\partial}{\partial t}(\rho \epsilon) + \frac{\partial}{\partial x_j}(\rho \epsilon u_j) = \frac{\partial}{\partial x_j}\left[\left(\mu + \frac{\mu_t}{\sigma_\epsilon}\right)\frac{\partial \epsilon}{\partial x_j}\right] + \rho C_1 S \epsilon - \rho C_2 \frac{\epsilon^2}{k + \sqrt{v\epsilon}} + C_{1\epsilon}\frac{\epsilon}{k}C_{3\epsilon}G_b + S_\epsilon \tag{5}$$

The SST k–ω model works well in areas near and far from the wall, and it can be used at low and high Reynolds numbers. It is more nonlinear than the k–ε model and has more difficulty in converging. The model provides a better prediction of flow separation than most Reynolds-averaged Navier–Stokes (RANS) models, which accounts for its good performance with adverse pressure gradients and is why it is frequently applied in aerodynamics. The turbulence kinetics is expressed as (Menter,1994)

$$\frac{\partial}{\partial t}(\rho k) + \frac{\partial}{\partial x_i}(\rho k u_i) = \frac{\partial}{\partial x_j}\left[\Gamma_k \frac{\partial k}{\partial x_j}\right] + \tilde{G}_k - Y_k + S_k \tag{6}$$

The specific dissipation rate is expressed as

$$130 \qquad \frac{\partial}{\partial t}(\rho\omega) + \frac{\partial}{\partial x_i}(\rho\omega u_i) = \frac{\partial}{\partial x_j}\left[\Gamma_\omega \frac{\partial\omega}{\partial x_j}\right] + G_\omega - Y_\omega + D_\omega + S_\omega \qquad (7)$$

2.3 Aero-acoustic formulation

Proudman (1952) applied Lighthill's acoustic theory to complete flow fields for the first time to derive the
135   noise generated from isotropic turbulence with low Mach numbers (M_t) and high Reynolds numbers.
However, the noise source generated by turbulent flow can be described as: (Lilley,1994)

$$p_A = \alpha_\varepsilon \rho_0 \varepsilon M_t^5 \qquad (8)$$

Where p_A, α_ε, and ρ_0 represent acoustic power, density of the far field, and an empirical constant (=0.1),
respectively. The turbulent M_t can be expressed as:

$$140 \qquad M_t = \frac{\sqrt{2k}}{\alpha_0} \qquad (9)$$

Where α_0 is the sound speed and k is the turbulence kinetic energy. It should be noted that this sound source
model assumes isotropic turbulence and only considers the energy of turbulent disturbances. Although it
cannot provide sound sources on the frequency spectrum, it is sufficient to evaluate the magnitude of the
noise and the results of subsequent noise reduction. On the other hand, the turbulent boundary layer generated
145   by the motion of an object will also produce noise sources on the object surface due to its disturbances. The
magnitude can be described as: (Curle,1955)

$$P_A = \int_S I\,dS \qquad (10)$$

Where P_A, I, and S are the acoustic power, sound intensity, and control surface on the moving object,
respectively. I can be expressed as:

$$150 \qquad I = \frac{A_c}{12\rho_0 \pi a_0^3}\overline{\left(\frac{\partial p}{\partial t}\right)^2} \qquad (11)$$

Where A_c is the correlation area. Generally, the noise generated from the blade surface is the main source of
noise, while the noise caused by turbulence is relatively small. Therefore, this study mainly focuses on the
noise generated by the blade.

155

2.4 CFD model

The Darrieus H-VAWT considered in this study had three blades, each with a S4415 airfoil shape, chord
length of 0.7 m, height of 5.5 m, and rotation radius of 2.235 m, as shown in Fig. 1(a). For the CFD model,
all of the blades were included in the computational domain, and the blade surfaces were set as stationary
160   walls for the boundary condition. To simulate the rotation of a VAWT, the computational domain was divided
into a rotating region and outer-flow region. As shown in Fig. 1(b), the rotating region was a dynamic mesh
that rotated at a frequency of 60 rpm in the shape of a vertical cylinder with a radius of 3 m and height of 6.5
m, and it included the three blades. The interface between the rotating region and outer-flow region was set
to the interface to ensure the continuity of the velocity and pressure between them. The geometric shape of
165   the outer-flow region should have little influence on the results because it is almost unaffected by the blades.
Figure 1(c) shows the outer-flow region; to simplify the mesh generation process, it was set as a horizontal
cylinder with a length of 40 m and radius of 5 m, where the top surface was set as the velocity inlet with a

standard wind speed of 12 m/s, the bottom surface was set as the pressure outlet with a pressure of 0 Pa, and the side surfaces were set to the symmetric boundary condition.

170
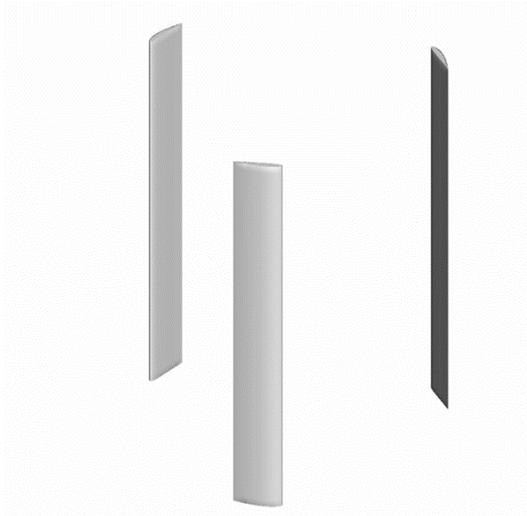
(a)
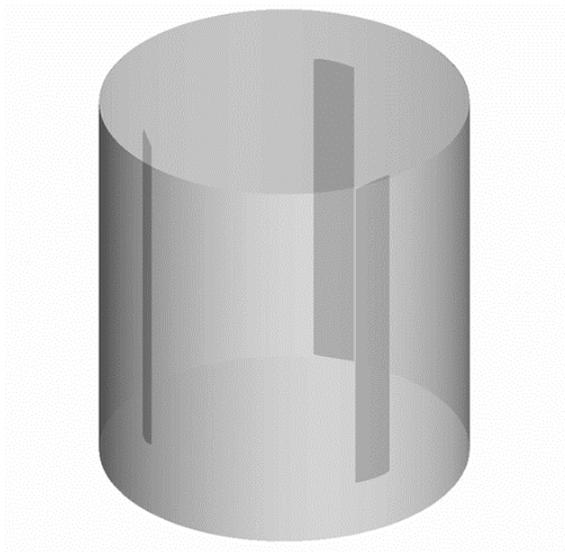
(b)
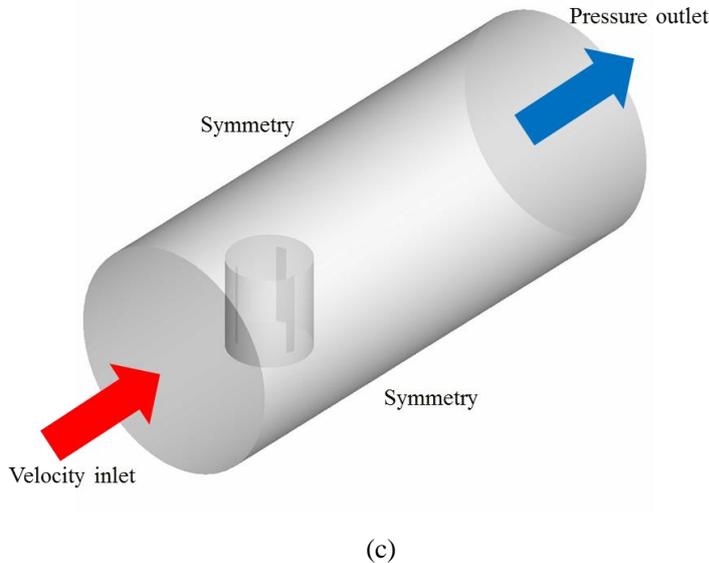
175

(c)

Figure 1: CFD model: (a) blade geometry, (b) rotating region, and (c) outer-flow region.

2.5 Mesh division

180 The momentum equation has a significant impact on the wind turbine torque. Thus, both the pressure and
velocity were discretized by using the second-order upwind scheme, and the SIMPLE algorithm was used to
couple the pressure and velocity. The turbulent kinetic energy and dissipation were discretized by using the
first-order upwind scheme. The time was discretized by using an implicit first-order differential equation
with a time step of 0.01 s. Spatial discretization is more complex because the flow field has different
185 characteristic lengths inside and outside the boundary layer. Therefore, the entire domain was divided into
three regions, all with different mesh sizes: the near-wall region, rotating region, and outer-flow region. The
near-wall region was the first mesh layer on the blade surface, and the mesh needed to be very dense to
facilitate the simulation of the velocity gradient and shear stress on the wall surface. The rotating region also
required a dense mesh to capture the wake and vortex formed after the airflow passed around the blade. The
190 outer-flow region was not affected by the blades, nor did it affect the blades. Thus, a coarser and unstructured
tetrahedral mesh could be used here. As shown in Fig. 2, the mesh sizes in the near-wall and rotating regions
were varied to evaluate the effect on the simulation results. The mesh type was not changed. An unstructured
mesh was used in the outer-flow region (Fig. 2(a)), and a higher-quality structured mesh was used in the more
complex rotating region (Figs. 2(a)–(d)). Table 1 presents the characteristic lengths of the four mesh sizes in
195 the near-wall and rotating regions. According to ASME standard (ASME V&V 20-2009), the characteristic
length of the mesh should be varied by about 1.3 times to evaluate the significance of different mesh sizes.

200

205

	(a)	(b)
	(c)	(d)
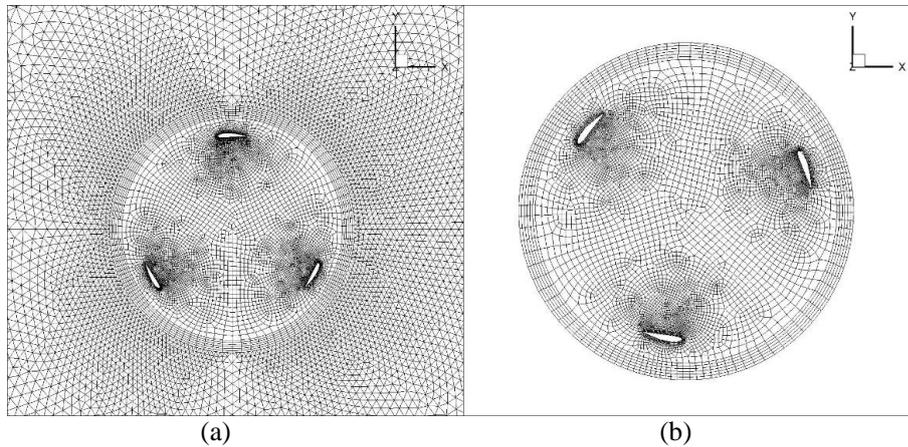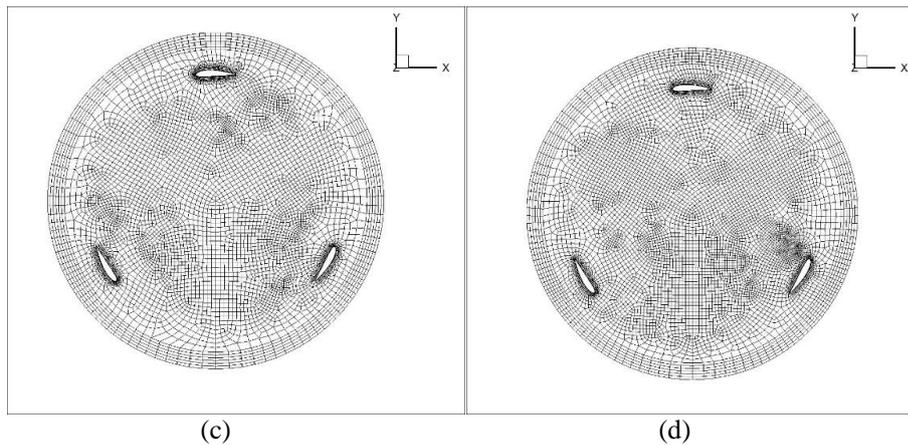
Figure 2: Divisions of (a) Mesh 1, (b) Mesh 2, (c) Mesh 3, and (d) Mesh 4.

210 **Table 1. Characteristic lengths of different meshes in each region.**

	Near-wall region (m)	Rotating region (m)	Outer-flow region (m)
Mesh 1	0.01	0.1	1
Mesh 2	0.003	0.1	1
Mesh 3	0.003	0.08	1
Mesh 4	0.003	0.06	1

3. Results and Discussion

215   CFD was used to simulate the torque and acoustic power distributions of a small VAWT in a standard wind speed 12 m/s and rotational speed 60 rpm in this study. The effects of the mesh and turbulence models were analyzed, and the best combination was applied to analyzing the flow field and identifying mechanisms for torque reduction and increased noise. Finally, three commonly used noise reduction techniques were evaluated for their effectiveness.

3.1 Effects of the mesh and turbulence models

220   Figure 3(a) shows the results of the mesh independence test. T is the time for one rotation. The predicted torque was quite sensitive to the mesh size, which could cause differences of over 50%. Fortunately, mesh independence could still be achieved by adjusting the mesh size in different regions, and mesh independencewas achieved with Mesh 3 and Mesh 4. Similar results were obtained for the predicted acoustic power on the blade, as shown in Fig. 3(b). Mesh 3 and Mesh 4 resulted in nearly identical predictions, so
225 Mesh 3 was selected for subsequent analysis because it had a smaller grid number and thus was less computationally intensive. Figure 3(c) shows that the torque predicted by the realizable k–ε and SST k–ω turbulence models were very similar. Both models obtained three peaks and valleys in one cycle, and the corresponding time points were almost identical except that the maximum value predicted by the realizable k–ε turbulence model was 11% higher than that predicted by the SST k–ω turbulence model. In addition, the
230 realizable k–ε turbulence model predicted a time-averaged torque of 227.7, which was slightly higher than the value of 207.2 predicted by the SST k–ω turbulence model. However, the two turbulence models showed significant differences in the predicted acoustic power, as shown in Figure 3(d) The time-averaged energy predicted by the realizable k–ε turbulence model was 57% higher than that predicted by the SST k–ω turbulence model. However, from an acoustic point of view, the difference between the two predictions was
235 about 1.9 dB, which is still acceptable. Previous studies have shown that the SST k–ω turbulence model has a higher tolerance for $y+$ and is more suitable for the geometry of different noise reduction techniques. (Menter, 1994; Menter, 2012) Therefore, the SST k–ω turbulence model was selected for subsequent analyses in this study.

240

(a)

(b)

(c)   (d)
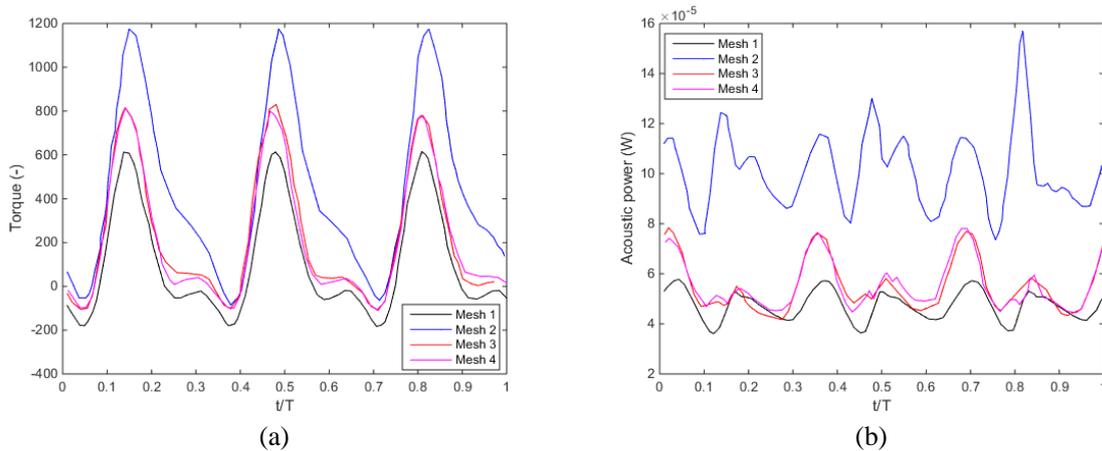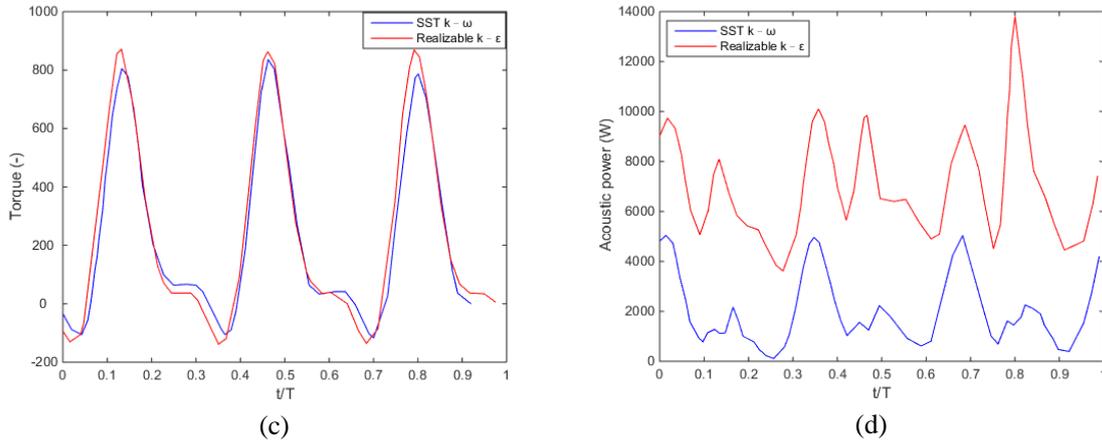
Figure 3: Effects of the mesh on the predicted (a) torque and (b) acoustic power. Effects of the turbulence model on the predicted (c) torque and (d) acoustic power.

245

3.2 Simulation without noise reduction

Figure 4(a) shows the predicted torque and noise for one cycle without noise reduction. The time-averaged
torque and noise sources on the blade surface were 207.2 and 5.8×10^{-5} W, respectively. These values were
250   used as benchmarks for evaluating the noise reduction techniques. The maximum noise coincided with the
minimum torque while the maximum torque increased noise to a much lesser extent than the minimum torque.
This phenomenon was further analyzed by the pressure and streamline distributions on the cross-section
combined with the turbulent kinetic energy distribution to further understand the characteristics of the flow
field. Figures 4(b) and (c) show the pressure distributions and streamlines at $t/T = 0.70$ and 0.82, respectively.
255   The wind flowed from left to right, and the blade rotated counterclockwise. At $t/T = 0.70$, the attack angles
of the three blades were −132°, −12°, and 108°. When air passed over the blade with an attack angle of −132°,
a vortex was generated behind the inner edge, which caused a low pressure zone that made it difficult for the
blade to rotate. Similarly, when the air passed over the blades with attack angles of −12° and 108°, high
pressure zones were generated in front that made it difficult for the blades to rotate. This resulted in a negative
260   torque, which means that an external force was needed to maintain the rotational speed. Because of the
symmetry of the three blades, this phenomenon also occurred at $t/T = 0.04$ and 0.37. At $t/T = 0.82$, the attack
angles of the blades were −55.2°, −175°, and 64.8°. For the blade with an attack angle of −55.2°, the airflow
generated a relatively high pressure on the outside and a large low pressure zone on the inner leading edge,
which drove the blade to produce a positive torque. No significant pressure differences were observed for the
265   blades with attack angles of −175° and 64.8°. The noise source caused by turbulence was proportional to the
fifth power of the turbulent kinetic energy. Therefore, the turbulent kinetic energy distribution could be used
to further analyze the noise caused by the flow field, as shown in Fig. 4(d). At $t/T = 0.70$, the vortex generated
on the inner edge of the blade with the −132° attack angle not only reduced the torque of the wind turbine
but also generated a large amount of turbulent kinetic energy, which produced the largest noise source. The
270   opposing distributions of torque and noise suggest that the VAWT can be designed to enhance torque and
reduce noise simultaneously.
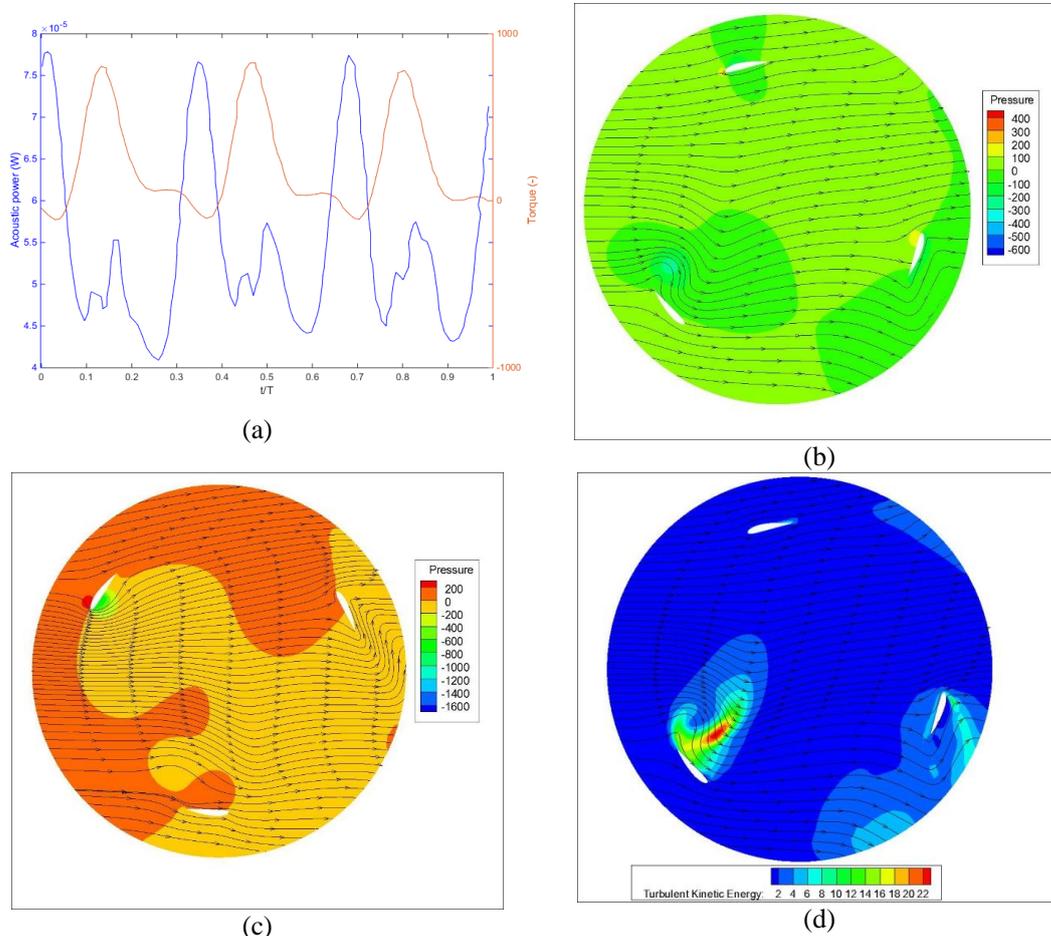
Figure 4: Simulation results without noise reduction: (a) comparison between the acoustic power and torque, pressure distributions and streamlines at (b) $t/T = 0.70$ **and (c) t/T = 0.82, and (d) turbulent kinetic energy distribution at** $t/T = 0.7$**.**

3.3 Simulation with noise reduction

Three commonly used noise reduction techniques were considered: a mask, deflector, and wall roughness. Mesh 3 and the SST k–ω turbulence model were used under the same wind speed and rotational speed conditions as for the simulation without noise reduction. The simulated torque and blade acoustic power were compared with the benchmark values to evaluate the effectiveness of each noise reduction technique.

3.3.1 Mask

Installing a mask on the upper and lower ends of a blade surface prevents sharp angles that cause strong separation or vortices. In this study, a mask with a long axis of 1.2 m and short axis of 0.5 m was installed at the upper and lower ends of the blades, as shown in Fig. 5. Figure 6(a) shows that installing the mask decreased the average torque by 40% to 124. However, Fig. 6(b) shows that the mask did not result in a corresponding decrease in the noise. The average acoustic power after installation was 6.34×10^{-5} W, which

290 is a 16% increase. As discussed in Sect. 3.2, the noise source was the vortex generated inside the blade after the blade cut through the wind field. Therefore, adding a mask at both ends not only failed to reduce noise but also increased the area of friction with the air, which actually increased the noise and resistance.
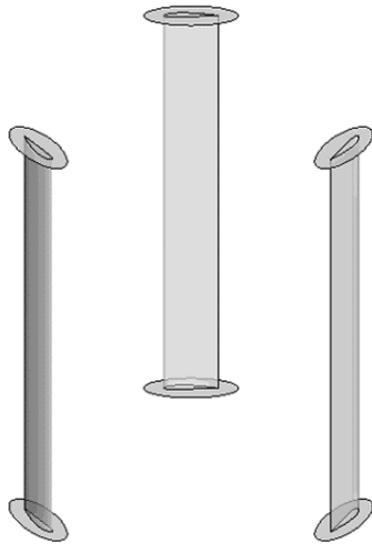
Figure 5: Geometric design of the mask.

(a)   (b)
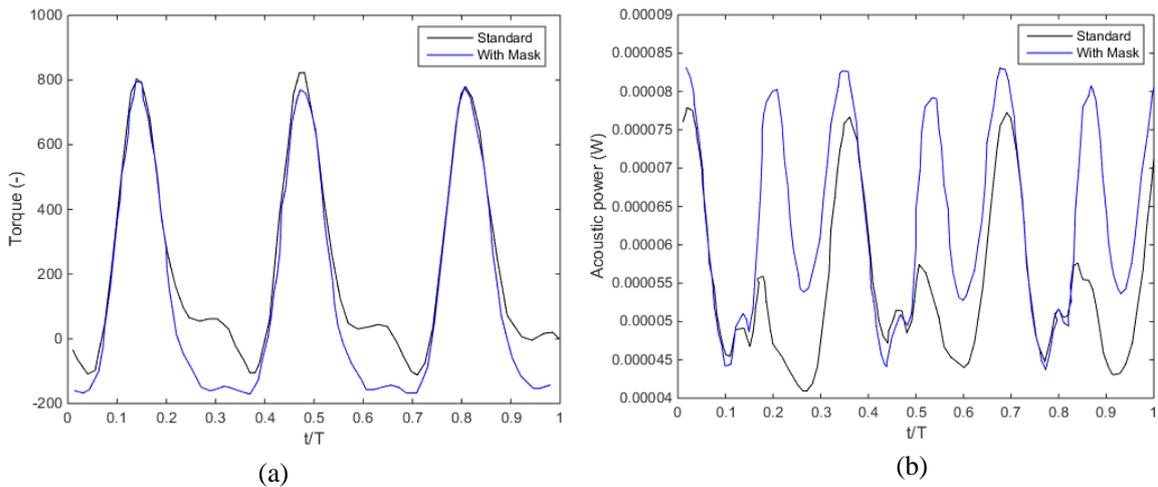
295 **Figure 6: Effects of a mask on the (a) torque and (b) acoustic power.**

3.3.2 Deflector

Figure 7 shows the deflector, which is a rectangular baffle with a length of 0.1 m, width of 0.2 m, and spacing of 0.2 m. Figures 8(a) and (b) show the effects of installing the deflector on the torque and blade noise, respectively. Installing the deflector increased the average torque by 169% to 564 and decreased the

300 blade noise by 98% to 7.86×10^{-7} W. Figure 8(c) shows the streamlines and pressure distribution after the deflector was installed when the torque was at its minimum (i.e., $t/T = 0.7$). Compared to the pressure

distribution without the deflector (Fig. 4(b)), the vortex at the inner edge of the blade with an attack angle of −132° detached further away from the blade surface, which resulted in a less significant impact on the blade surface and enhanced the torque. Figure 8(d) shows the turbulence kinetic energy distribution at this time

305 and clearly indicates that the vortex separated from the blade. In contrast, the turbulence distribution without the deflector (Fig. 4(c)) shows that the vortex adhered closely to the inside of the blade and continued to affect the blade surface. However, installing the deflector did generate greater turbulent kinetic energy throughout the rotation area, which increased the turbulent noise and thus needed to be evaluated. Figure 8(e) shows the noise energy caused by turbulence in the rotating region. Installing the deflector increased the

310 average turbulent noise kinetic energy about 10.6 times to 2.95×10^{-6}. After the installation of the deflector, the main noise-generating mechanism changed from boundary layer disturbance to turbulence generated noise. However, the noise generated by turbulence after deflector installation was still an order of magnitude less than the blade noise before installation. This indicates that installing a deflector would be effective for noise reduction.

315
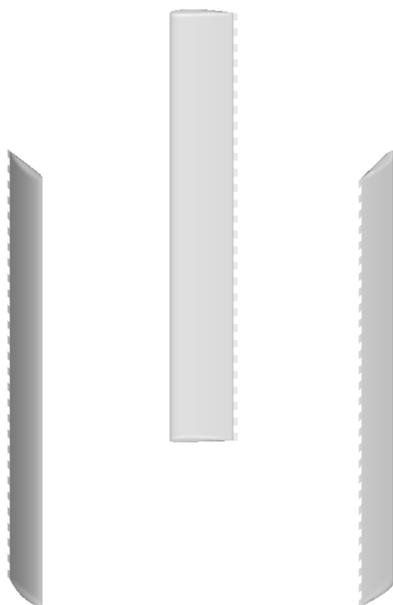
Figure 7: Geometric design of the deflector.

(a)

320

(b)
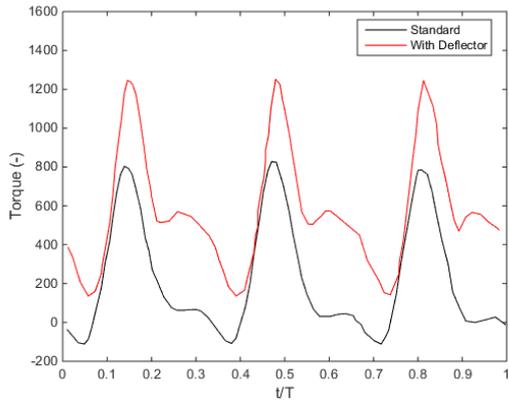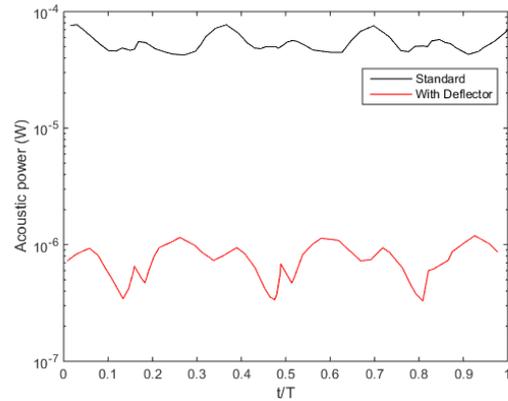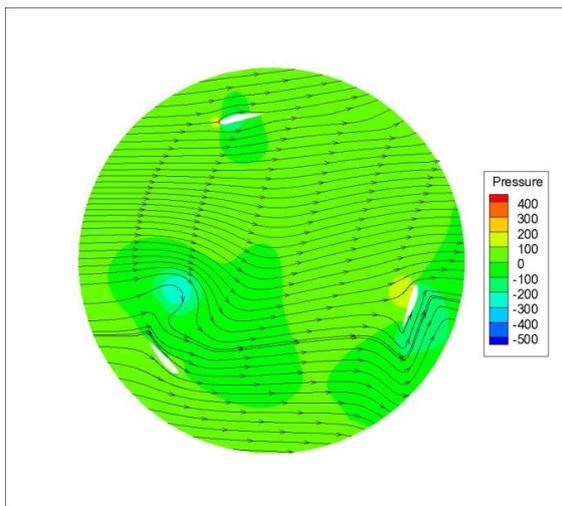
(c)
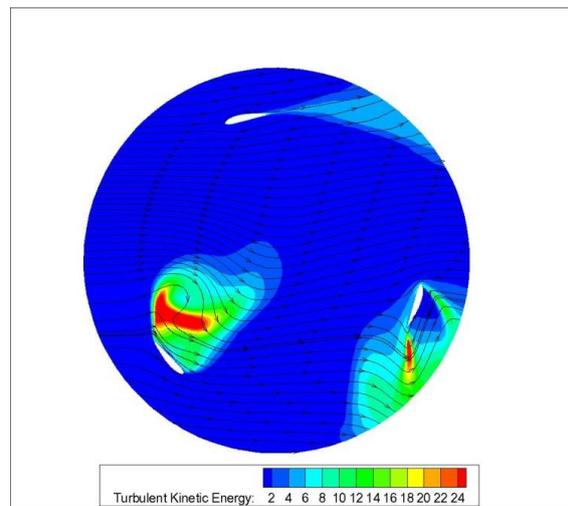
(d)
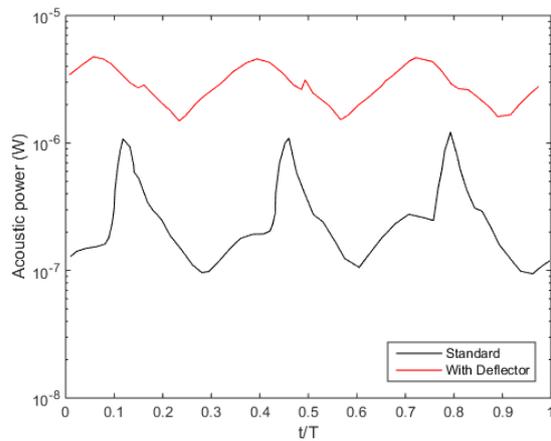
(e)

Figure 8: Effects of a deflector on the (a) torque, (b) blade surface noise, (c) pressure distribution and streamlines at *t/T* = 0.7, (d) turbulent kinetic energy distribution at *t/T* = 0.7, and (e) turbulent flow noise.

325

3.3.3 Wall roughness

To achieve noise reduction, the blade surface can be roughened to be similar to that a golf ball. This suppresses the boundary layer separation and reduces the vortex scale, which reduces noise emissions. In this study, the boundary conditions for the rough blade surface were described by modifying the wall function to account for greater wall shear stress on rough surfaces:

$$u^+ = \frac{1}{\kappa}\log y^+ - \Delta B \tag{12}$$

where κ and ΔB are the Von Karman constant and roughness function. With different roughnesses, ΔB can be expressed as

$$\Delta B = \begin{cases} 0 & \text{for } K_s^+ \leq 2.25 \\ \frac{1}{\kappa}\ln\left(\frac{K_s^+ - 2.25}{87.75} + C_s K_s^+\right) \times \sin\left[0.4258\left(\ln K_s^+ - 0.811\right)\right] & \text{for } 2.25 \leq K_s^+ \leq 90 \\ \frac{1}{\kappa}\ln\left(1 + C_s K_s^+\right) & \text{for } K_s^+ > 90 \end{cases} \tag{13}$$

where K_s^+ is the non-dimensional roughness

$$K_s^+ = \frac{\rho K_s u^*}{\mu} \tag{14}$$

In Eq. (14), the roughness height was assumed to be 0.01 m. Figures 9(a) and (b) show the effects of a rough surface on the torque and blade noise, respectively. Increasing the roughness decreased the torque by about 50% from 209 to 100. However, the noise on the blade surface increases significantly from 5.45×10^5 to 1.9×10^{-3} W. Figure 9(c) shows that the maximum acoustic power of the turbulent flow decreased slightly. These results show that increasing the roughness reduced the boundary layer and vortex, but the main noise source became the oscillating interaction between the blade surface and the air rather than the oscillation of the turbulence and vortex.

(a)

(b)

345

(c)
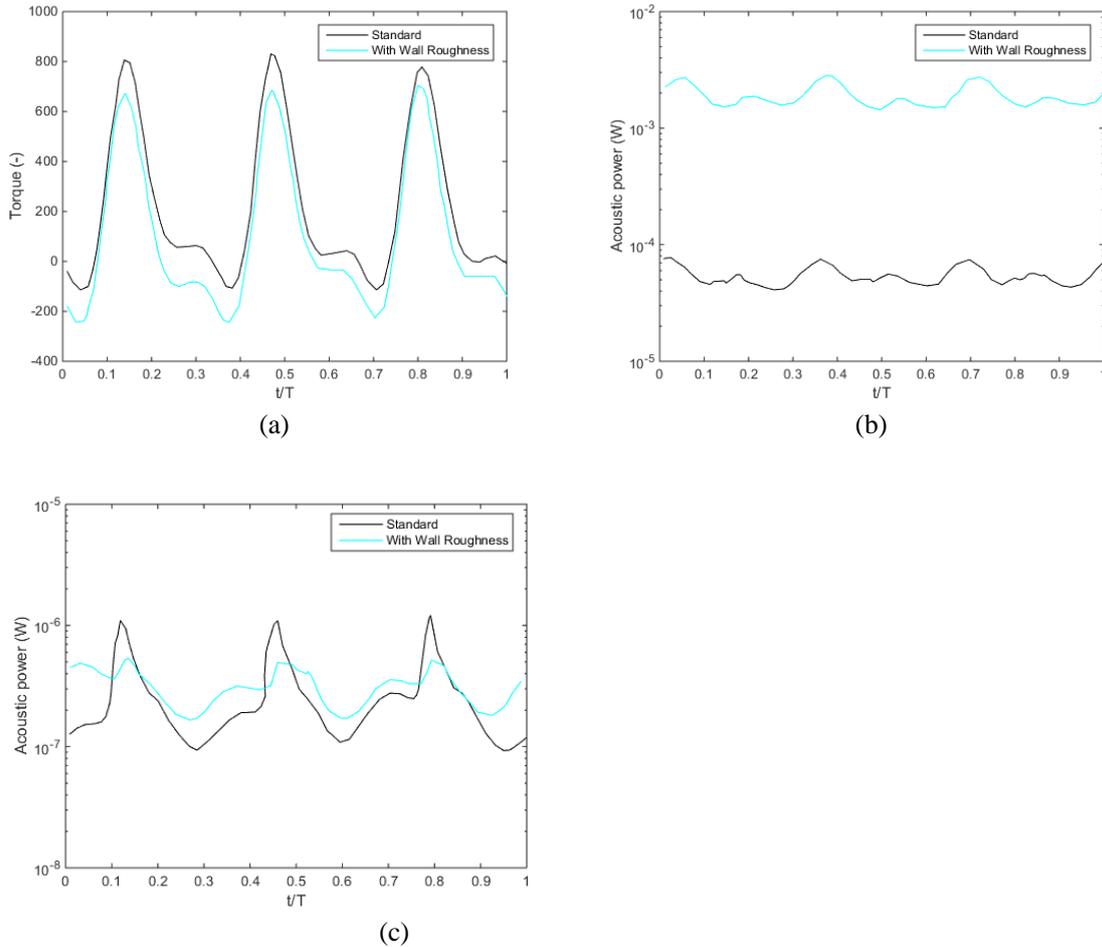
Figure 9: Effects of the wall roughness on the (a) torque, (b) blade surface noise, and (c) turbulent flow noise.

4. Conclusion

350   With the rapid advancement of computer science and technology, the use of CFD technology has become increasingly prevalent as a formidable means of exploring the aerodynamics of wind turbines. However, improving the performance and reducing the noise of VAWTs remains a difficult task due to their complex aerodynamic characteristics. ANSYS FLUENT is a powerful tool for investigating the aerodynamic and aeroacoustic behaviors of wind turbines, offering advantages such as low cost and providing a high
355   visualization effect of the distribution. In this study, CFD simulations were performed to evaluate the effects of different noise reduction techniques on a small VAWT suitable for urban settings. A suitable mesh size and a turbulence model were determined, and the VAWT was initially evaluated to identify the reasons for torque reduction and noise increase. The choice of turbulence model is related to the operating condition and tolerance for y+ of the wind turbine. The SST k–ω turbulence model can better predict the flow field
360   characteristics around the wind turbine with or without noise reduction techniques. Then, three different noise reduction techniques were tested, and adding a deflector was found to increase the overall torque and decrease

the blade noise. It also increased the turbulence noise, but this was still about 90% lower than the original blade noise. After installing the deflector, the torque of the blades increases by 169%, the acoustic power of the blades decreases by 98%, and the turbulent acoustic power increases up to 964%. Thus, the deflector is a suitable noise reduction technique for small VAWT. The results of this study can serve as an important reference for other wind turbines under similar operating conditions and may contribute to the wider spread of small VAWTs in an urban setting. The aerodynamic performance enhancement of the small VAWT using the deflector can be done as future work, and it can be installed on the passage between the buildings and along the rooftop with a Fluid-Structure-Interaction study. This study is limited to only a numerical study using CFD techniques and steady-state simulations. Any airflow unsteadiness and variations in the intermittency and variability of wind speed and rotational speed were not considered in detail. Furthermore, the impacts of uniform and non-uniform building arrangements in an urban area are not yet taken into consideration. Higher-order models with unsteady wind conditions, tubercle amplitude-wavelength optimization, experimental analysis, and design optimization of the wind turbine parameters will be the future studies.

Competing interests

The contact author has declared that none of the authors has any competing interests.

Acknowledgments

Support from the Atomic Energy Council (AEC), Taiwan is acknowledged.

References

Shoutu Li et al.: Experimental investigation on noise characteristics of small scale vertical axis wind turbines in urban environments, Renewable Energy., 200, 970–982, https://doi.org/10.1016/j.renene.2022.09.099, 2022.

Lighthill Michael James.: On sound generated aerodynamically I. General theoryProc, R. Soc. Lond, A211564–587, http://doi.org/10.1098/rspa.1952.0060, 1952.

Proudman I.: The generation of noise by isotropic turbulence Proc. R. Soc. Lond, A214119–132, http://doi.org/10.1098/rspa.1952.0154, 1952.

A. Pradera, G. Keith, F. Jacobsen, N. Gil-Negrete and A. Rivas.: A numerical study of fluid flow past a circular cylinder at Re = 3900 and a practical approach to noise prediction, 14th International Congress on Sound and Vibration, 2007.

A. Tadamasa and M. Zangeneh.: Numerical prediction of wind turbine noise, Renewable Energy., 36, 7, 1902-1912, https://doi.org/10.1016/j.renene.2010.11.036 , 2011.

N. N. Sorensen, J. A. Micheksen and S. Schreck.: Navier-Stokes Predictions of the NREL Phase VI Rotor in the NASA Ames 80ftx120ft Wind Tunnel, Wind Energy., 5, 151-169, https://doi.org/10.1002/we.64, 2002.

Maizi M, Mohamed M, Dizene R and Mihoubi M.: Noise reduction of a horizontal wind turbine using different blade shapes. Renewable Energy., 117, 242-256, https://doi.org/10.1016/j.renene.2017.10.058, 2018.

400   Deshmukh S, Bhattacharya S, Singh V, Kumar R.: Aerodynamic and aeroacoustic study of horizontal axis wind turbine with winglets. B.Tech. Thesis; Department of Mechanical Engineering, MNNIT Allahabad, 2018.

Mohamed, M. H.: Reduction of the generated aero-acoustics noise of a vertical axis wind turbine using CFD (Computational Fluid Dynamics) techniques, Energy., 96, 531-544,
405   https://doi.org/10.1016/j.energy.2015.12.100, 2016.

Botha, J. D. M., A. Shahroki, and H. Rice.: An implementation of an aeroacoustic prediction model for broadband noise from a vertical axis wind turbine using a CFD informed methodology, Journal of Sound and Vibration., 410, 389-415, 10.1016/j.jsv.2017.08.038, 2017.

Gabriel Naccache, Marius Paraschivoiu.: Development of the Dual Vertical Axis Wind Turbine Using
410   Computational Fluid Dynamics. ASME. J. Fluids Eng., 139(12), 121105, https://doi.org/10.1115/1.4037490, 2017.

Gabriel Naccache, Marius Paraschivoiu.: Parametric study of the dual vertical axis wind turbine using CFD. J. Wind Eng. Ind. Aerodyn., 172, 244-255, https://doi.org/10.1016/j.jweia.2017.11.007, 2018.

Klein, L., Gude, J., Wenz, F., Lutz, T., and Krämer, E.: Advanced computational fluid dynamics (CFD)–
415   multi-body simulation (MBS) coupling to assess low-frequency emissions from wind turbines, Wind Energ. Sci., 3, 713–728, https://doi.org/10.5194/wes-3-713-2018, 2018.

Nyborg, C. M., Fischer, A., Réthoré, P.-E., and Feng, J.: Optimization of wind farm operation with a noise constraint, Wind Energ. Sci., 8, 255–276, https://doi.org/10.5194/wes-8-255-2023, 2023.

Abreu, R., Peter, D., and Thomas, C.: Reduction of wind-turbine-generated seismic noise with structural
420   measures, Wind Energ. Sci., 7, 1227–1239, https://doi.org/10.5194/wes-7-1227-2022, 2022.

W.-H. Chen, J.-S. Wang, M.-H. Chang, et al., Efficiency improvement of a vertical-axis wind turbine using a deflector optimized by Taguchi approach with modified additive method, Energy Convers. Manag., 245, 114609, https://doi.org/10.1016/j.enconman.2021.114609, 2021.

Ji Yao, Weibin Yuan, jianliang Wang, Jianbin Xie, Haipeng Zhou, Mingjun Peng, Yong Sun.: Numerical
425   simulation of aerodynamic performance for two dimensional wind turbine airfoils, Procedia Engineering., 31, 80-86, https://doi.org/10.1016/j.proeng.2012.01.994, 2012.

Moath N. Zaareer, Abdel-Hamid Ismail Mourad, Tariq Darabseh, Kassim Abdullah, Mostafa S.A. ElSayed.: Aeroacoustics wind noise optimization for vehicle's side mirror base, International Journal of Thermofluids., 18, 100332, https://doi.org/10.1016/j.ijft.2023.100332, 2023.

430   Shih,T.-H., Liou, W. W. Shabbir, A. Yang, Z. and Zhu, J.: A New - Eddy-Viscosity Model for High Reynolds Number Turbulent Flows - Model Development and Validation, Computers Fluids., 24(3). 227–238, https://doi.org/10.1016/0045-7930(94)00032-T, 1995.

Menter F. R.: Two-Equation Eddy-Viscosity Turbulence Models for Engineering Applications, AIAA Journal., 32(8), 1598–1605, https://doi.org/10.2514/3.12149, 1994.

435   Lilley, G.M.: The radiated noise from isotropic turbulence. Theoret. Comput. Fluid Dynamics 6, 281–301, https://doi.org/10.1007/BF00311842, 1994.

Curle, N.: The Influence of Solid Boundaries upon Aerodynamic Sound. Proceedings of the Royal Society of London. Series A, Mathematical and Physical Sciences., 231(1187), 505–514, http://www.jstor.org/stable/99804, 1955.

440 The American Society of Mechanical Engineers.: Standard for Verification and Validation in Computational Fluid Dynamics and Heat Transfer, ASME V&V 20-2009, 2009.

Menter, F. R.: Zonal two equation k-ω turbulence models for aerodynamic flows, AIAA Paper 93- 2906, https://doi.org/10.2514/6.1993-2906, 2012.